IMPACT OF CROSS WINDS IN POLAR REGIONS ON GOCE ACCELEROMETER AND GRADIOMETER DATA

Nadja Peterseim[1], **Anja Schlicht**[2], **Claudia Stummer**[1], **and Weiyong Yi**[1]

[1]*Institut für astronomische und physikalische Geodäsie, Technische Universität München, Germany*
[2]*Forschungseinrichtung Satellitengeodäsie, Technische Universität München, Germany*

ABSTRACT

GOCE V_{yy} gravity gradients show a signature around the magnetic poles when compared to corresponding reference gradients computed with EGM08. These signatures have no gravitational origin. This hints at an insufficiency of the GOCE processing chain. In this work we are able to show that cross winds have a significant impact onto common mode accelerations of GOCE. This impact can clearly be related to the signature in the V_{yy} gravity gradients in the time domain, which is further evidence for a necessary improvement of the inverse calibration matrices (ICMs). According to the reprocessing of the GOCE data, as carried out by the European Space Agency (ESA), we vary the scale factor within the ICMs which is mainly contributing to the signals observed around the magnetic poles.

Key words: GOCE; thermospheric cross winds; gradients; Inverse Calibration Matrix.

1. INTRODUCTION

The Gravity field and steady-state Ocean Circulation Explorer (GOCE) was launched March 17 in 2009 and is collecting information about Earth' gravity field since then with unprecedented accuracy. The key instrument of GOCE is the onboard gradiometer, consisting of three accelerometer pairs, whereas one pair is mounted on each of the three orthogonally aligned axes of the gradiometer. Every accelerometer is located 0.25 m from the origin of the gradiometer axes. The measurements of the accelerometers are used to derive common mode (CM) and differential mode (DM) acceleration data. Non-gravitational, linear accelerations are represented within the CM accelerations. These accelerations are due to forces being exerted onto the spacecraft such as atmospheric drag, which is being compensated by GOCE's onboard drag-free control (DFC) system in along track. The main target of the satellite's mission, the determination of Earth' gravity field, is mainly depending on the gathering of gravity gradients (GG), which are derived from DM accelerations [1].

Of importance to this work is a new processing of raw instrument time series to calibrated products (Level 0 to Level 1b). This calibration is originally carried out by the European Space Agency's (ESA) Payload Data Segment (PDS). The internal calibration of the raw instrument data, the derivation of the so-called inverse calibration matrices (ICMs; [1]), is one of the major tasks of the processing. These ICM contain the imperfections of GOCE's gradiometer such as scale factors, misalignments of the accelerometers and non-orthogonalities of the axes.

The linear accelerations acting upon the spacecraft can be described by the mean of the accelerations of one accelerometer pair (CM accelerations). With equation 1 CM accleeartions can be derived, with k, l the number of the accelerometer and i the measurement direction. GG ought to be only found within DM accelerations, describing the opposite to CM (cf. equation 2), the half of the differemce between two accelerations in one direction.

$$a_{c,k,l,i} = \frac{1}{2}(a_{k,i} + a_{l,i}) \tag{1}$$

$$a_{d,k,l,i} = \frac{1}{2}(a_{k,i} - a_{l,i}) \tag{2}$$

In principle, the CM accelerations should not affect the GG measurements, however, due to the small imperfections within the gradiometer, CM accelerations might leak into the GG. Therefore, CM and DM accelerations need to be clearly separated by the ICMs.

A hint at an imperfectly derived ICM can be found, when normal calibrated V_{yy} gradients as observed by GOCE are compared to computed V_{yy} gradients from EGM08 up to degree and order 210 (O-C, observed minus computed), which are rotated into GOCE's gradiometer reference frame (GRF), filtered into the gradients nominal measurement bandwidth (MBW; [2]; cf. figure 1). The GRF is defined as follows: x is defined as the axis pointing from the gradiometers origin to the satellites front and hence in flight trajectory (with a slight deviation), z is nadir pointing (referred to as radial), and y is the axis perpendicular to the other two to complete the triad (referred to as cross track). Here, a clear signal can be found around the magnetic poles, whereas the signal in the south appears to be dominant.

Proc. of '4th International GOCE User Workshop', Munich, Germany
31 March – 1 April 2011 (ESA SP-696, July 2011)

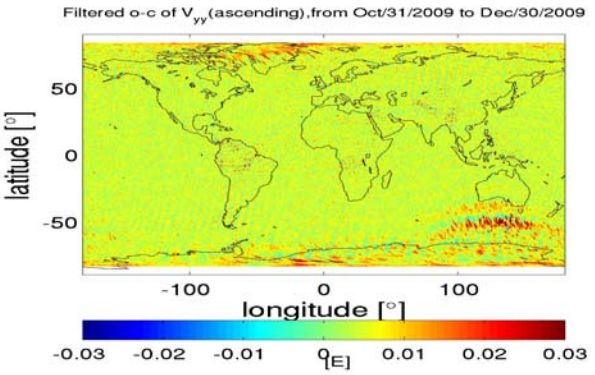

Figure 1. V_{yy} O-C gradients, with EGM08 as reference model (d/o 210), 31 October to 31 December 2009.

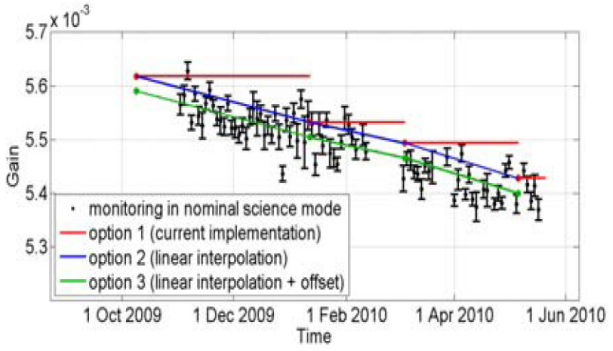

Figure 2. Time series of the ICM element $dSF25_y$. The calibration parameter shows a drift of -29 ppm/month (Courtesy Christian Siemes, ESA, [3]).

In this work, first adjustments corresponding to the ESA's reprocessing in calibration are performed. Every element of the ICM has been linearly interpolated inbetween the ICM values from the previous and following calibration phase [3]. Furthermore, the ICM element corresponding to the differential scale factor along the gradiometer arm 25 ($dSF25_y$) has been varied by numerous factors. This element separates the DM accelerations of accelerometer units 2 and 5 and the cross track CM accelerations (cf. equation 3 and 4). Especially for $dSF25_y$ a nearly linear drift can be discovered for ICMs of different epochs (cf. figure 2). An offset in the mentioned d_{25} element can be derived by monitoring parameters in science mode as discussed by [3].

$$ICM = \begin{bmatrix} C & D \\ D & C \end{bmatrix} \tag{3}$$

$$a_{d,i,j} = D_{i,j} \cdot \widetilde{a}_{c,i,j} + C_{i,j} \cdot \widetilde{a}_{d,i,j} \tag{4}$$

After calibration the DM accelerations still include, apart from GG, accelerations due to centrifugal force (ω^2) acting upon the spacecraft, which needs to be subtracted, according to the following equations (for diagonal elements on the ICM):

$$V_{xx} = -\frac{2a_{d,1,4,x}}{L_x} - \omega_y^2 - \omega_z^2, \tag{5}$$

$$V_{yy} = -\frac{2a_{d,2,5,y}}{L_y} - \omega_x^2 - \omega_z^2, \tag{6}$$

$$V_{zz} = -\frac{2a_{d,3,6,z}}{L_z} - \omega_x^2 - \omega_y^2. \tag{7}$$

With $L_{x,y,z}$ describing the distance between the two accelerometers in direction x, y and z. In order to derive the gradients accurately, the angular velocity needs to be known. For deriving the angular velocity the precise attitude of the satellite needs to be known. The attitude is derived by star sensor data, STR, and the gradiometer itself, as STR data are less accurate for higher frequencies [2]. In order to find the best angular rate over the entire frequency range, a combination of STR and gradiometer data needs to be carried out - this process is being referred to as the angular rate reconstruction (ARR), and it is nominally being carried out in the time domain by means of Kalman filtering [1]. However, in this work we used the approach as described in Stummer et al. (2011; [2]), who carries out the ARR by means of Wiener filtering.

In order to understand the signals corresponding to the variations in $dSF25_y$, the following paragraph shall comment on the structures being observed in the auroral ovals (cf. figure 1). Using the accelereomter data of the CHAllenging MiniPayload (CHAMP) mission it was possible to determine cross wind patterns over the polar regions [4]. A fast day-to-night flow with mean speeds surpassing 600 m/s in the dawn sector has been discovered over the northern polar cap. Over the southern polar cap the winds have a lower velocity and the high speed winds focus more on the auroral oval structure (cf. figure 3). Furthermore, a thermospheric mass density over the polar regions, especially concerning the auroral ovals, has been discovered in CHAMP altitudes, which is 20-30% higher during night hours local time (LT) than the estimation of commonly used models [5].

Only varying $dSF25_y$ is a rather unusual approach. In

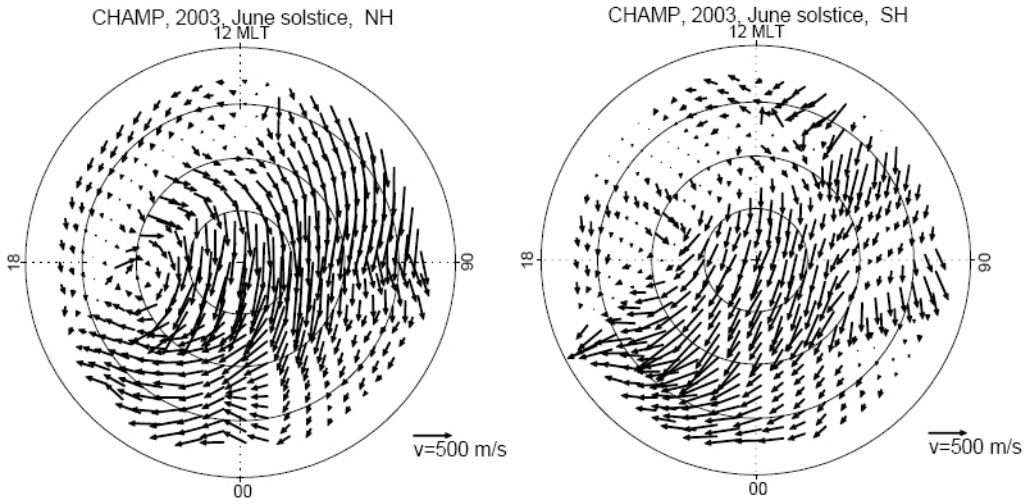

Figure 3. Distribution of mean thermospheric wind vectors over northern (right, summer) and southern hemisphere (right, winter), magnetic coordinates, June solstice (Courtesy Hermann Lühr, GFZ Potsdam, [4]).

fact, all scaling factor parameters change from ICM to ICM determination, whilst the parameters for non-orthogonalities and misalignments remain rather stable. However, element $dSF25_y$ is showing a strong drift over time and has an additional offset (cf. figure 2). Therefore, as a first appraoch, in this study only this special element within the ICM shall be varied, also as elements $dSF25_y$ and $dSF14_x$ are most critical to GG determined by GOCE [6]. Variations are carried out as an addition of the numbers mentioned later in this work onto the original scaling factor. All elements, indluding $dSF25_y$ of each part of the ICM have been adjusted by a linear interpolation for every sample of the epoch.

2. TIME DOMAIN DATA

Following the introduced processing chain the observed signal concerning the regions over the poles can be first seen in the cross track CM accelerations. In order to emphasise the impact of this signal, we compared each CM acceleration with the corresponding V_{yy} gradients derived from the reference model EGM08 up to degree and order 210 subtracted from the corresponding V_{yy} gradients as observed by GOCE. In figures 4 and 5 we compared a signature which can be typically found south of Australia corresponding the described auroral oval region when GOCE is flying with ascending node, which is always at dusk in local time (LT), as GOCE is flying a sun-synchronous orbit. All further plots throughout this paper correspond to an ascending node. In figure 4 the CM acceleration can be observed, whereas the introduced signature concerning the polar region consists of the major down-upward peaks. In figure 5 the corresponding detrended V_{yy} O-C gradients are shown. Here, blue represents the regularly derived ICM with ARR derived by means of Wiener filtering, green represents an offset applied in ICM element $dSF25_y$ of $-2.75 \cdot 10^{-5}$ as determined by [3], red an offset in the same ICM element of $-3.375 \cdot 10^{-5}$, cyan an offset of $-4 \cdot 10^{-5}$ and magenta an offset of $-6 \cdot 10^{-5}$. It can clearly be seen that the structure in O-C GG has an inverted behaviour to the structure in CM accelerations, indicating a coupling of the CM and DM accelerations. The figure has been split in two parts in order to emphasise the behaviour of a changing scale factor with respect to the regular ICM. In the lower image of the figure it is obvious that the magenta sample already inverted the signal majorly, except for the sharp peak. Whenever the scaling factor in $dSF25_y$ has been varied, also a linear interpolation between all elements of the ICM with the ICM of the following epoch has been carried out for every sample. In figure 5, upper image, it is obvious, that the overall signature has been smoothened using the described approach compared to a regularly applied ICM, following a smooth curve. However, the sharp spike, that can be observed at $3.685 \cdot 10^4$ seconds is getting smaller, but is not eliminated (both parts of figure 5).

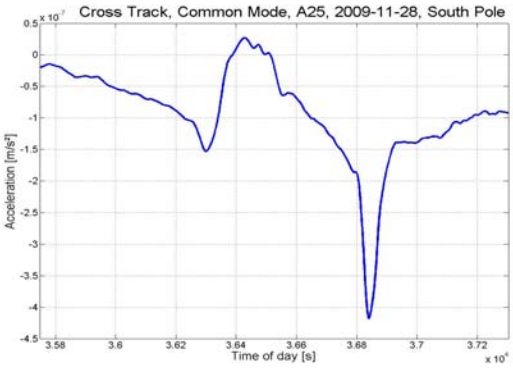

Figure 4. Cross wind signal in CM acceleration at South Pole.

Moreover, in figures 6 and 7 similar plots can be seen, focusing on the auroral oval region over the North Pole. Here (cf. figure 7), in contrast to the South Pole, no sudden, sharp spikes can be observed. The colours in the figure correspond to the colours in figure 5. In this image it is also clearly visible, that the signature has faded with the applied approach and has been replaced by a smooth curve.

3. GLOBAL DATA

The described signal can also be observed when the V_{yy} O-C GG are interpolated onto a global grid. For all following figures the data has been filtered with a bandpass filter of 1 mHz to 10 mHz as this bandwidth corresponds strongly to the effects focused on in this study. Figure 8 is representing a mean for November 2009. In figure 8a the impact of the signatures into the V_{yy} O-C GG with a regular ICM can be seen (corresponding to blue O-C GG in figures 5 and 7). Clearly, the structures of the auroral ovals can be observed with absolute amplitudes of up to $2 \cdot 10^{-11}\ 1/s^2$. Furthermore, a strong signal can be seen following the magnetic equator, which is most likely caused by ionospheric turbulences acting upon the satellite. For figure 8b to 8d we vary the scale factor of ICM y-element d_{25} from $-2.75 \cdot 10^{-5}$ over $-3.375 \cdot 10^{-5}$ to $-4 \cdot 10^{-5}$. For the signature concerning the South Pole it is obvious, that the signal is decaying, with one small artefact remaining right south of Australia. Apparently,

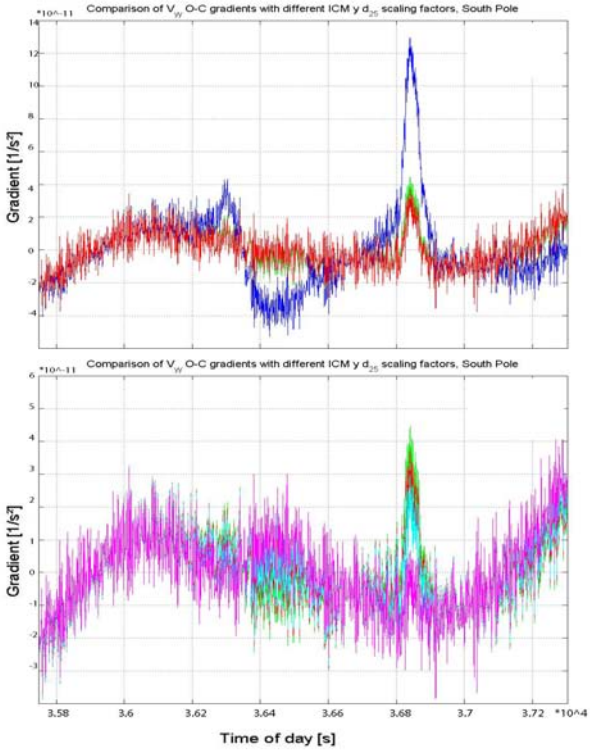

Figure 5. Corresponding (cf. fig. 4 detrended V_{yy} O-C gradients with different $dSF25_y$ ICM variations. Blue: regular ICM, green: SF = $-2.75 \cdot 10^{-5}$, red: SF = $-3.375 \cdot 10^{-5}$; cyan: $-4 \cdot 10^{-5}$; magenta: $-6 \cdot 10^{-5}$.

for the North Pole the variations of the scale factors are getting too strong and the signal is inversing. On the signal concerning the magnetic equator the variation of the scale factor, as well as the linear fitting, has obviously very small impact. For a $dSF25_y$ addition of $-6 \cdot 10^{-5}$ (not displayed) both sigantures at the poles are inversed for most parts, except for the artefact south of Australia, which vanished completely.

Time variability

In figure 9, the corresponding plot to figure 8.b of a mean for December 2009 is displayed. It is obvious, that the impact of the approach on the V_{yy} GG residuals is getting smaller, which hints at an insufficiency of the linear interpolation between the ICM elements of different, suc-

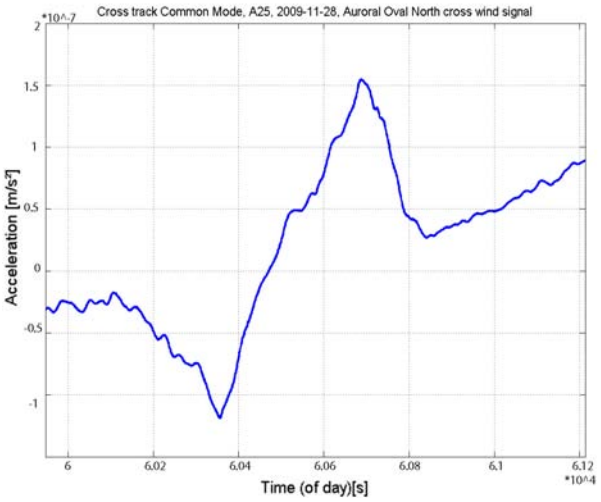

Figure 6. Cross wind signal in CM acceleration at North Pole.

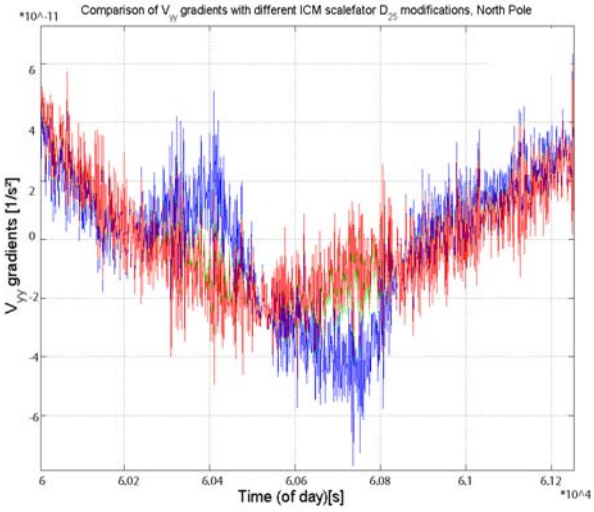

Figure 7. Corresponding (cf. fig. 6 detrended V_{yy} O-C gradients with different $dSF25_y$ ICM variations. Blue: regular ICM, green: SF = $-2.75 \cdot 10^{-5}$, red: SF = $-3.375 \cdot 10^{-5}$.

cessive ICMs.

4. DISCUSSION

When the satellite is crossing the area over the South Pole, the wind strikes its cross track plane. This wind describes a nearly homogenous linear acceleration. This becomes obvious as the signal can be clearly observed within the CM accelerations in cross track. The shape of the O-C GGs relate to the shape of CM accelerations, which are shaped by cross winds, and therefore the anomaly within the O-C GGs must be correlated to an insufficient calibration.

In addition to this, the center of pressure (CoP) and the center of mass (CoM) of the satellite are not located in the same place, but have an offset of

$$CoM - CoP = \begin{pmatrix} -0.30 \\ 0.01 \\ 0 \end{pmatrix} m. \qquad (8)$$

This means the CoP is located slightly behind the CoM for aerodynamic stability [7]. If CoM and CoP are not located in the same position, however, a homogenous exerted force onto the spacecrafts plane will evoke a rotation of the satellite. In this case a rotation in yaw, around the z axis, is enforced. The satellite's onboard attitude and orbit control system (AOCS) is in charge to maintain the nominal attitude and orbit. As attitude is being controlled by onboad magnetic torquers (MTQ), which act in correspondence with Earth' magnetic field, which means that in the proximity of the magnetic poles the control around the yaw axis (Z-axis) is weak (magnetic field lines are vertical), which corresponds to a slight inability of the magnetic torquers to control the yaw-rotation in the auroral oval. This means, that a possible influence by roation into the gradients cannot be excluded, however, the rotation must be corrected with the variation of other ICM elements.

Furthermore, in figure 3 it can be deduced, that there is a stronger wind blowing in the dusk/ evening LT hours that in the hours from morning to early afternoon. This contributes to the fact, that the signatures in the auroral ovals are most likely to be seen, when GOCE is flying with ascending node rather then descending node, due to GOCE's sun-synchronous orbit.

We showed that we were able to weaken the structures observed near the poles in the V_{yy} gradients. However, we also discovered, that changing only one scale factor within the ICM, despite the linear interpolation for all ICM-elements, is not optimal for both poles, as the signal

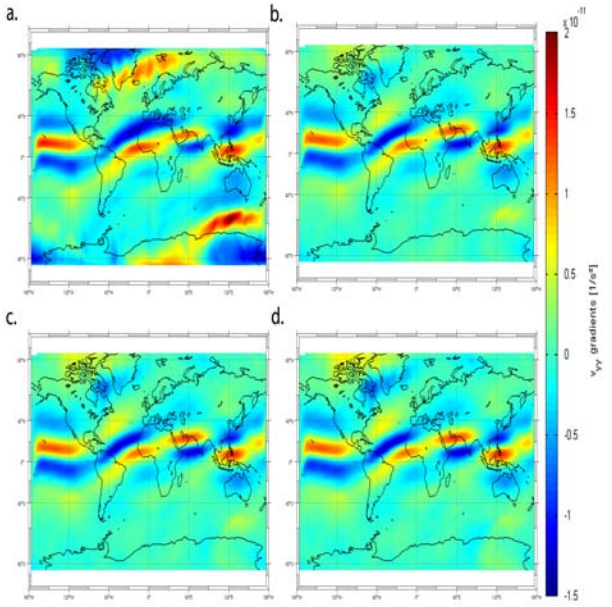

Figure 8. Mean O-C gravity gradient data of November 2009 interpolated on a global grid with y d_{25} variations. a: regular ICM; b: SF = $-2.75 \cdot 10^{-5}$; c: SF = $-3.375 \cdot 10^{-5}$; d: SF = $-4 \cdot 10^{-5}$.

in the North is already inversing for a scale factor whilst the signal in South is still decaying. Even the signal in regarding the South Pole is not reacting homogeneously, which is becoming obvious when $dSF25_y$ has been increased by $-6 \cdot 10^{-5}$. The smoothly varying parts are being inverted whereas the strong peak observed is not fully eliminated. This also contributes to the fact, that the signal observed around the equator is affected slightly by variatons of this specific scale factor, but is not being weakened. An influence of the rotational acceleration with a non-linear dependence on the cross winds in correlation with the yaw angle of GOCE could be the cause.

Moreover, we could show that a linear interpolation between each element of the following ICMs of two epochs is not optimal, as the applied offset onto the scaling factor has a stronger impact at times, where the data is closer to the actual determined ICM for the given epoch. This could also correspond to figure 10 as the lines for North and South pole offset determinations show no smooth linear drift, but rather a linear drift overlaid by a noisy signal. Another hypothesis is that the dependency on the North and South Pole signatures could be due to Earth' magentic field itself.

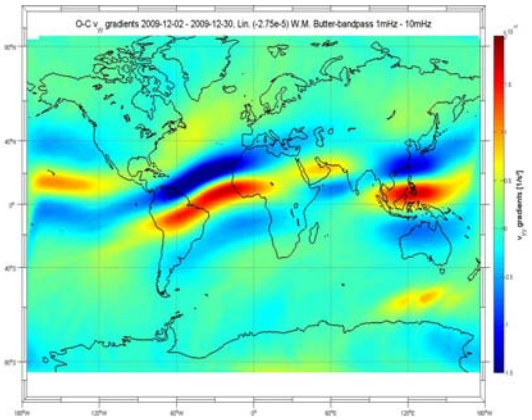

Figure 9. Mean O-C gravity gradient data of December 2009 interpolated on a global grid with $-2.75 \cdot 10^{-5}$ added to $dSF25_y$.

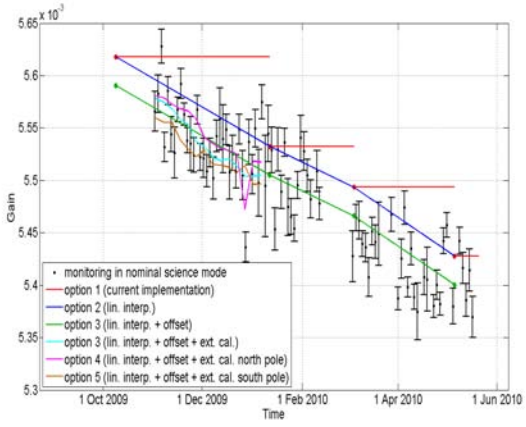

Figure 10. Offset individually derived for regions concerning North (magenta) and South pole (brown) (Courtesy Christian Siemes, ESA, [6]).

And we could show that a linear interpolation between each element of the following ICMs of two epochs is not optimal, as the applied offset onto the scaling factor has a stronger impact at times, where the data is closer to the actual determined ICM for the reference epoch. This could also correspond to figure 10 as the lines for North and South pole offset determinations show no smooth linear drift.

5. OUTLOOK

Further studies concerning the introduced difference of the North and South Poles are planned. Especially a possible influence of Earth' magnetic field on GOCE regarding this aspect shall be investigated.

Another aspect worth being studied are the rotations of the satellite in the corresponding regions itself and how other ICM scaling factors may contribute helping to improve the GG determined by GOCE. Understanding this could possibly help to eliminate the siganture around the equator.

Also, the results of this study should be validated with data and ICMs from other epochs.

ACKNOWLEDGEMENTS

We would like to thank ESA and the HPF team for supplying us with the data this study is based upon and all the helpful discussions.

Furthermore, we would like to thank Hermann Lühr from Helmholtz-Zentrum Potsdam - Deutsches GeoForschungsZentrum Potsdam (GFZ Potsdam) for his overall support, concerning the understanding of the interactions between thermospheric characteristics and spacecrafts in Low Earth Orbit heights.

Last but not least we want to thank Christian Siemes from the European Space Research Institute (ESRIN), ESA, for the helpful discussions regarding the ICMs and specifically the single elements within them.

REFERENCES

[1] Cesare C., Catastini G., 1973, Gradiometer On-Orbit Calibration Procedure Analysis. Technical Note to ESA, GO-TN-AI-0069, Issue 4, Alenia Aerospazio

[2] Stummer C., Fecher T., Pail R., 2011, Alternative method for angular rate determination within the GOCE gradiometer processing, J. Geod. (in print), doi:10.1007/s00190-011-0461-3

[3] Siemes Ch., Haagmans R., Kern M., Drinkwater M., Plank G., Floberghagen R., 2010, Monitoring and validation of GOCE calibration parameters (G31A-0792), Poster presented at AGU in San Francisco, USA.

[4] Lühr H., Rentz S., Ritter P., Liu H., Häusler K., 2007, Average thermospheric wind patterns over the polar regions, as observed by CHAMP, Ann. Geophys., 25, 1093-1101

[5] Liu H., Lühr H., Henize V., Köhler W., 2005, Global distribution of the thermospheric total mass density derived from CHAMP, J. Geophys. Res., Vol. 110, A04301, doi:10.1029/2004JA010741

[6] Siemes Ch., 2011, personal correspondence.

[7] Fehringer M., 2010, E-Mail correspondence.